HHS Public Access

Author manuscript

Mol Psychiatry. Author manuscript; available in PMC 2018 February 05.

Published in final edited form as:

Mol Psychiatry. 2017 October ; 22(10): 1464–1472. doi:10.1038/mp.2016.233.

Ankyrin-G isoform imbalance and interneuronopathy link epilepsy and bipolar disorder

Angel Y. Lopez, BS[1], **Xinjun Wang, PhD**[2], **Mingxuan Xu, PhD**[3], **Atul Maheshwari, MD**[3,4], **Daniel Curry, MD**[5], **Sandi Lam, MD**[5], **Adekunle M. Adesina, MD**[6], **Jeffrey L. Noebels, MD, PhD**[1,3,4], **Qian-Quan Sun, PhD**[2], and **Edward C. Cooper, MD, PhD**[1,3,4]

[1]Departments of Molecular and Human Genetics, Baylor College of Medicine, Houston, TX, USA

[2]Department of Neuroscience, University of Wyoming, Laramie, WY, USA

[3]Neurology, Baylor College of Medicine, Houston, TX, USA

[4]Neuroscience, Baylor College of Medicine, Houston, TX, USA

[5]Department of Neurosurgery, Texas Children's Hospital, Houston, TX, USA

[6]Department of Pathology, Texas Children's Hospital, Houston, TX, USA

Abstract

ANK3, encoding the adaptor protein Ankyrin-G, has been implicated in bipolar disorder by genome wide association studies. *ANK3* has multiple alternative first exons, and a bipolar disorder-associated *ANK3* variant has been shown to reduce expression of exon 1b. Here we identify mechanisms through which reduced *ANK3* exon 1b isoform expression disrupts neuronal excitation-inhibition balance. We find that parvalbumin interneurons and principal cells differentially express *ANK3* first exon subtypes. Parvalbumin interneurons express only isoforms containing exon 1b, whereas excitatory principal cells express exon 1e alone, or both 1e and 1b. In transgenic mice deficient for exon 1b, parvalbumin interneurons lack voltage-gated sodium channels at their axonal initial segments and have increased firing thresholds and diminished action potential dynamic range. These mice exhibit an *Ank3* gene dosage-dependent phenotype including behavior changes modeling bipolar disorder, epilepsy, and sudden death. Thus, *ANK3*'s important association with human bipolar susceptibility may arise from imbalance between ankyrin-G function in interneurons and principal cells and resultant excessive circuit sensitivity and output. Ankyrin-G isoform imbalance is a novel molecular endophenotype and potential therapeutic target.

Address for Correspondence: Edward C. Cooper, MD, PhD, Departments of Neurology, Neuroscience, and Molecular and Human Genetics, Baylor College of Medicine, 1 Baylor Plaza, M.S. NB302, Houston TX 77030, office: 713-798-4939, fax: 713-798-3464, ecc1@bcm.edu.

CONFLICT OF INTEREST

The authors have nothing to disclose.

Supplementary information is available at *Molecular Psychiatry's* website.

INTRODUCTION

Depression, bipolar disorder (BD), and epilepsy are common, chronic, episodic brain disorders(1–3), sharing many features, including very high social cost and elevated suicide risk(4–6). Mood disorder is the most frequent major comorbidity associated with epilepsy, and the risk of exhibiting BD symptomatology in epilepsy patients has been estimated at 10–12%(7). Conversely, patients with BD are reported to have an approximately two to four-fold increased risk of epilepsy(8–10). Identification of Mendelian epilepsy genes has enabled studies of pathophysiological mechanisms and driven efforts towards mechanism-based epilepsy therapy(11). Although BD is highly heritable(12), its genetic and phenotypic complexity makes the task of identifying underlying biological mechanisms especially challenging even when association signals are known(13).

ANK3 is a leading candidate gene in BD, implicated by multiple genome-wide association and targeted replication studies in diverse populations(14–19). *ANK3* uses alternative transcriptional start sites, alternative first exons, and additional downstream alternative exons to produce multiple isoforms of its protein product, ankyrin-G (AnkG) (Figure 1a, b)(20, 21). Alternative *ANK3* first exons 1a/1a′, 1e, and 1b encode AnkG N-terminal peptide sequences, here called NT1, NT2 and NT3 (Figure 1A, B; Supplementary Figure 1). In neurons, AnkG clusters voltage-gated sodium (Na_V) and KCNQ2/3 potassium channels at axonal initial segments and nodes of Ranvier (NRs), enabling action potential (AP) generation and conduction(23–25). The *ANK3* 1e and 1b alternative first exons encode highly conserved AnkG N-terminal peptides (Supplementary Figure 1) that control the ratio of neuronal Na_V and KCNQ2/3 channels binding to AnkG, and hence, excitability(26). Remarkably, six different neuronal Na_V and KCNQ channels bound near the AnkG N-terminus are encoded by genes mutated in human Mendelian epilepsy syndromes (*SCN1A, SCN2A, SCN8A, SCN1B, KCNQ2, KCNQ3*)(27). Drugs that block Na_V channels (i.e., carbamazepine, lamotrigine, valproic acid) or promote opening of KCNQ2/3 channels (valproic acid)(28) are used widely for both epilepsy and BD(29). Thus converging human genetic, molecular, and clinical pharmacological evidence makes *ANK3* an appealing candidate for BD and mood disorder-epilepsy comorbidity.

We noted that many of the BD-associated *ANK3* variants lie within candidate cis-regulatory regions between exons 1e and 1b (Figure 1a)(30, 31). Furthermore, recent experiments in human and mouse provide hints that decreased expression of *ANK3* isoforms containing exon 1b may increase BD susceptibility, whereas decreased exon 1e expression may be protective(21, 32). The rs1938526 single nucleotide variant, associated in several independent studies with increased BD risk, has been shown to correlate with reduced human brain levels of exon 1b-containing mRNA(21, 33). Mice heterozygous for exon 1b deletion have a behavioral phenotype characterized by reduced anxiety and increased motivation for reward at baseline, which transitions to depression-related features after repetitive stress, modeling decompensation in BD(32). The rs41283526 SNP, which lies downstream of exon 1e and causes impaired splicing and reduced mRNA expression, was found be protective both for BD (odds-ratio, 0.31) and schizophrenia (odds-ratio, 0.21; Figure 1a) (33). However, neurophysiological mechanisms explaining why altered *ANK3*

exon 1b and exon 1e expression might influence susceptibility to BD and epilepsy are unknown.

We investigated the expression and function of AnkG isoform subfamilies defined by alternative first exons and alternative N-termini, in mouse and human. We obtained robust molecular, electrophysiological, and behavioral evidence that AnkG exon 1b expression controls the excitability of parvalbumin (PV)-expressing fast-spiking inhibitory neurons(34) that are known to control output gain in neocortical microcircuit responses(35, 36). Our findings provide clear, conceptually simple links between AnkG expression, excessive output in neuronal circuits, epilepsy, and emotional disorder.

MATERIALS AND METHODS

Animals

C57BL/6J Ank3-exon1b(20) and conditional *Ank3* knockout(37) founder mice were provided by Vann Bennett. All mutant mice used in experiments were produced by crosses of animals heterozygous at all alleles in order to generate test mice and littermate controls. Mice expressing tdTomato in PV interneurons were generated as described(38). NT3-*Ank3* mutant animals expressing tdTomato in PV interneurons were used for slice electrophysiology and electroencephalography; their genotypes are *Ank3-1b*$^{+/+}$*-PVcre-tdTom*, *Ank3-1b*$^{KO/+}$*-PVcre-tdTom*, *Ank3-1b*$^{KO/KO}$*-PVcre-tdTom* (here called *Ank3-1b*$^{+/+}$*-PVtom*, *Ank3-1b*$^{KO/+}$*-PVtom* and *Ank3-1b*$^{KO/KO}$*-PVtom* mice). This combination of alleles allowed for the constitutive *Ank3* exon1b KO mice to express tdTomato fluorescence in only PV interneurons. Conditional *Ank3* knockout of AnkG in PV interneurons used mice with lox-P sites flanking *Ank3* exons 22 and 23, which are constitutive in all large AnkG isoforms. These mice were crossed with *PV-cre;tdTom* mice to generate PV-specific *Ank3* knockout mice expressing tdTomato (here called *Flox-Ank3*$^{KO/KO}$). Restricted tdTomato expression in PV interneurons was verified by comparing tdTomato fluorescence and PV immunofluorescence using confocal microscopy. Primers for genotyping *Ank3-1b* alleles(20) and *Flox-Ank3* alleles(37) were reported previously. Primers used for genotyping *PV-cre* (Jackson Labs, stock no. 008069) and *tdTomato* (Jackson Labs, stock no. 007905) mice were those recommended by The Jackson Laboratory catalogue. Mice used in immunostaining and EEG experiments were 6–8 weeks of age. Both sexes were used in all preliminary experiments and exhibited the same robust immunostaining pattern and EEG phenotypes. Subsequently, experiments quantifying staining intensity and EEG features were performed on male mice only. All animal procedures followed protocols approved by the IACUC committees of Baylor College of Medicine and the University of Wyoming.

Human tissue

Human brain samples were obtained under a protocol approved by the Baylor College of Medicine Institutional Review Board. Overlying neocortical tissue removed as part of routine care from patients undergoing surgery for epilepsy and tumors (ages 9–19 years) was used. Cortical tissue blocks (approximately 5 mm^3) were immersion fixed (4% PFA, 2 hours), located and oriented using surgical notes and the intact pial surface, embedded in OCT, cryosectioned (60 μm), and processed as described for mouse samples.

Materials

To generate an NT2-AnkG-GFP expression construct, we cloned *Ank3*-exon1e cDNA (Open Biosystems, catalogue #MMM1013-64925) into pEGFP-N1. Vann Bennett provided a rat NT3-AnkG270-GFP plasmid and affinity-purified rabbit anti-All AnkG antibodies (raised against a large C-terminus fusion protein). Isoform-specific rabbit antibodies against portions of the NT1-AnkG, NT2-AnkG and NT3-AnkG peptides were raised (YenZym, Inc., S. San Francisco, CA) and affinity-purified using methods described previously(22). Antigenic peptides used were derived from the human sequences, with a C-terminal cysteine residue added for conjugation: NT1 (NT1-AnkG residues 8–29): SPAGTEDSAPAQGGFGSDYSRSSRKSC; NT2 (residues 2–21): SEEPKEKPAKPAHRKRKGKKC; NT3 (residues 2–21): AHAASQLKKNRDLEINAEEEC. Purchased primary antibodies were mouse N-terminal isoform non-selective, called here "All AnkG" (IgG2a, clone N106/36; UC Davis/NIH NeuroMab Facility; Davis, CA), mouse anti-PV (IgG1, clone Parv-19, Sigma-Aldrich; St. Louis, MO), and mouse anti-PanNaV (IgG1, Sigma-Aldrich). Corresponding secondary antibodies were dylight488 donkey-anti-rabbit IgG (Jackson ImmunoResearch; West Grove, PA), AlexaFluor647-conjugated goat anti-mouse IgG1 (Invitrogen; Eugene, OR), AlexaFluor555-conjugated goat anti-mouse IgG2a (Invitrogen), and, for western blots, HRP-conjugated anti-rabbit IgG (Jackson).

Western blot

Forebrain and cerebellum were dissected from 3 P6 mice, homogenized (100 mg wet weight/ml) in buffer containing 40mM Tris-HCl (pH 7.4), 150mM NaCl, 1% Triton X-100 (Tx-100), 1x Complete protease inhibitor (Roche), and 1mM DTT. Proteins were denatured in SDS sample buffer, subjected to gel electrophoresis and transfer, and blotted using antibodies against NT2-AnkG, NT3-AnkG and AnkG C-terminus.

Transfection and immunostaining

Human embryonic kidney (HEK) 293 cells were cultured, transfected, and immunostained as described(22). All immunostaining steps were performed in parallel for genotypes being compared. Initial experiments determining conditions and setting assumptions of statistical tests were performed using 7 *Ank3-1b*$^{KO/KO}$ males, 2 *Ank3-1b*$^{KO/+}$ females, and 4 WT females. Final image collection for figures and quantification of results (except antibody validation shown in Supplementary Figure 2) was performed on male littermates: *Ank3-1b*$^{KO/+}$ (n=8) and wild type (WT) (n=17). Mice were deeply anesthetized using isofluorane and perfused with cold PBS followed by 4% paraformaldehyde. Brains were post-fixed (1.5 hr at 25°C) and embedded in OCT (Tissue-Tek, Torrance, CA). Cryosections (20 μm) were mounted on Superfrost Plus slides (Fisher; Waltham, MA). Human and mouse section staining protocols and HEK cell epifluorescence/brightfield imaging was performed as described(22). For dual labeling using PV and AnkG antibodies, conditions for optimal fixation (sufficient to preserve parvalbumin in the tissue, but weak enough to allow preservation of strong AnkG immunoreactivity) were developed transcardiac perfusion with 4% PFA in PBS, and sampling post-fixation durations of 0.5, 1, 1.5 and 2 hours. Results shown here used 1.5 hours, after which blocks were transferred to 30% sucrose overnight and embedded for later sectioning.

Confocal imaging and analysis

Images were collected using a Nikon C2 confocal microscope, 20x dry and 60X oil immersion planapo objectives, and NIS-Elements software (Nikon; Melville, NY). Brain regions were identified using a mouse brain atlas(39). For quantification experiments, slides were coded by one experimenter, and images were acquired and analyzed by another experimenter blinded to sample genotype. High-resolution image stacks (NA 1.4; xy = 0.06–0.09 μm; z interval = 0.238 μm; pinhole: 0.6–0.8 Airy unit) were acquired. The origin and distal tip of each AIS was carefully determined using maximal projection and 3D views (Supplementary Data movie 1). Only neurons whose somata, proximal dendrites, and AISs were entirely contained within the imaged volume were included in measurements of AIS size and labeling intensity. Using NIS-Elements tools, AIS labeling quantification was performed in parallel by two alternative approaches, an intensity threshold/region of interest (ROI) strategy, and a line sampling strategy described previously (23). These yielded very similar results and ROI measurements are reported here. Nested repeated-measures two-way ANOVA (6 AISs per mouse and four mice per genotype) was used to determine the significance of changes in PV interneuron labeling intensities in WT compared to *Ank3-1b*$^{KO/+}$ mice(Prism; GraphPad, La Jolla, CA).

Video-electroencephalography

Video-electroencephalography (video-EEG) monitoring was performed as described previously(38), at six to eight weeks of age, over a single, continuous 24-hour period for each animal. During manual video-EEG review, frequency of spikes (40 ms, 600 μV), cumulative spike-wave (SW) time, SW event frequency, and average event duration were measured. SW discharges were included in event calculations if they lasted ≥ 500 ms, had voltage amplitudes ≥2X the interictal baseline, and had frequencies of 5–9 Hz. Videos and simultaneous EEG were analyzed for corresponding behavioral changes. Group comparison statistical significance was tested using a nonparametric Mann-Whitney test (Prism).

Slice electrophysiology

Experiments were performed on *Ank3-1b*$^{KO/KO}$ and WT (n=9 for each genotype, 4 males and 5 females) at eight to ten weeks of age. Recordings were made by an investigator blinded to genotype. Mice were deeply anesthetized using isoflurane and decapitated. The brains were immediately removed and transferred into ice cold oxygenated slicing medium containing the following (in mM): 2.5 KCl, 1.25 NaH_2PO_4, 10 $MgCl_2$, 0.5 $CaCl_2$, 26 $NaHCO_3$, 11 glucose, and 234 sucrose. Thalamocortical slices (300 μm) were cut using a vibratome by methods optimizing preservation of thalamocortical and intracortical connections, as described (40, 41). Cut slices were rested in artificial cerebral spinal fluid (aCSF, in mM: 126 NaCl, 2.5 KCl, 1.25 NaH_2PO_4, 1.0 $MgCl_2$, 2.0 $CaCl_2$, 26 $NaHCO_3$, and 10 glucose, gassed with 95% O_2/5% CO_2, pH 7.4) at 35 °C for 1 hour. Slice electrophysiology and synaptic conductance calculation was performed as described previously (42). Initial analysis showed no sex differences, and in the results shown here, data for the two sexes are pooled.

Statistical procedures

Power analysis was performed using G*Power (Univ. of Dusseldorf) using estimates of effect size based on preliminary experiments. All calculated means are expressed ± the standard error of the mean.

RESULTS

Alternative N-termini define brain ankyrin-G subfamilies

To elucidate potential distinctive neural functions of AnkG subtypes, we generated NT1, NT2 and NT3 isoform-specific antibodies using sequences derived from human exon 1a/1a′, 1b, and 1e (Supplementary Figure 1). Control western blot and immunostaining using these antibodies demonstrated their specificity and utility (Supplementary Figure 2). In western blots against mouse brain proteins, NT2 and NT3 antibodies both detected the canonical AnkG 480, 270 and 190 kD polypeptides, consistent with previous mRNA studies in human and mouse(20, 21, 43). NT1 antibodies detected heterologously expressed protein well (Supplementary Figure 2a, 2c), but showed no reactivity against mouse brain tissue and, in particular, no staining of AISs (discussed below, Supplementary Figures 2i, 6d). By contrast, affinity-purified NT2 and NT3 antibodies showed widespread, overlapping, non-identical mouse brain regional immunolabeling patterns that were completely absent in samples reacted with pre-immune sera (Supplementary Figure 2f). In the cerebellar cortex, NT3 strongly labeled stellate, basket, Purkinje and granule cell AISs; transgenic mice lacking expression of NT3-AnkG exhibited complete loss of AnkG immunostaining from these cerebellar AISs. In cerebellar Golgi cells, AISs stained for NT2. No cerebellar AISs of wild type or mutant mice were labeled by NT1 (Supplementary Figure 2g–j)(20, 22).

NT3-AnkG role in forebrain PV interneurons

ANK3-exon1b mRNA is found in forebrain(21), but protein localization has not been previously shown. Staining with NT3-AnkG antibodies revealed widespread, regionally varied labeling (Supplementary Figure 3a–d). The frontal cortex, orbitofrontal cortex and anterior cingulate cortex showed especially strong labeling. Other areas of the limbic system, including the hippocampal dentate gyrus and amygdala, as well as the basal ganglia and the reticular thalamic nucleus, exhibited strong NT3-AnkG labeling. We systematically analyzed AnkG isoform expression in brain regions implicated in emotion processing in BD(44). In the hippocampus, labeling for NT2-AnkG was more conspicuous than for NT3-AnkG (Figure 1c, e). However, as in the cerebellum, higher resolution imaging revealed a striking, cell-type-specific pattern. NT2 and NT3 antibodies both strongly labeled AISs of dentate granule cells (DGCs; Figure 1d, f). AISs of hippocampal pyramidal cells were strongly labeled by NT2-AnkG antibodies and lacked NT3-AnkG staining (Figure 1c, e, g–j). However, a few AISs within and outside the pyramidal cell layer in all CA regions were strongly NT3-positive. Co-labeling and 3D-reconstruction (Supplementary Information, Movie 1) revealed that each CA region NT3-labeled AIS arose from a PV interneuron soma or proximal dendrite (n=46, Figure 1g, h) and that all PV interneuron AISs were NT2-negative (n=25, Figure 3i, j). This unexpected result led us to collect high-resolution images of PV interneuron AISs in other forebrain regions implication in emotional control, including the amygdala (n=27, Figure 2) and the orbitofrontal and anterior cingulate cortex

(n=54, Supplementary Figure 4). In these regions, all PV interneuron AISs were labeled only by NT3-AnkG (Figure 2b, c, f, g). Principal cells and non-PV interneurons stained for NT2-AnkG and NT3-AnkG in ratios that varied between neighboring cells within a circuit (Figure 3d, h; Supplementary Figure 4c, f). A striking exception to this pattern was found in the caudoputamen, where the medium spiny neurons, like hippocampal pyramidal cells, all labeled exclusively for NT2-AnkG (Supplementary Figure 5).

In mice, homozygous deletion of exon 1b (*Ank3-1b*$^{KO/KO}$) results in a complete loss of AnkG, Na_V channels and KCNQ2/3 channels at most cerebellar cortex AISs, including basket and stellate cells which are PV interneurons (Supplementary Figure 2e–g)(20, 22). Consistent with that, in *Ank3-1b*$^{KO/KO}$ mice, forebrain PV interneuron AISs were not detectable by AnkG or PanNa_V antibodies (data not shown). In heterozygous *Ank3-1b*$^{KO/+}$ mice, labeling for PanAnkG, NT3-AnkG, and PanNa_V was reduced by approximately half (Figure 1k, l). Reduced AIS length (Supplementary Figure 6b), and reduced labeling density both contribute to the overall reduction in total AnkG and PanNa_V labeling at PV cell AISs of *Ank3-1b*$^{KO/+}$ mice. PanAnkG and PanNa_V labeling of CA1 pyramidal neuron AISs was unchanged (Supplementary Figure 6a). NT1 and NT2 remained undetectable at *Ank3-1b*$^{KO/+}$ mouse CA1 PV interneuron AISs (n=18; Supplementary Figure 6c, d). Thus, reduced NT3 levels produce no effective compensatory expression of NT1 or NT2 isoforms in these cells.

NT3-AnkG in mouse and human neocortex

To examine ankyrin labeling in human brain, we focused on frontal or temporal cortex, as samples from these regions removed as part of neurosurgical care at our center could be immediately processed in parallel with mouse samples. In all layers of the mouse frontal cortex, pyramidal cell AISs are labeled for NT2 and NT3 (Figure 3a, b). Mouse frontal cortical PV interneuron AISs all stained strongly for NT3-AnkG (n=24) and undetectably for NT2-AnkG (n=19; Figure 3c, e). Cingulate cortex pyramidal cells AISs were heterogeneous in their NT2 and NT3 labeling strength (Figure 3d, f). In orbitofrontal cortex as well, PV interneuron AISs labeled robustly for NT3-AnkG (n=5) and lacked NT2-AnkG (n=6; Supplementary Figure 6a, b, d, e), but pyramidal cells showed heterogeneity of NT2- and NT3-AnkG staining (Supplementary Figure 6c, f). In human frontal cortex, AnkG isoform expression exhibited the same neuronal cell type-dependent pattern: PV interneuron AISs stain strongly for NT3-AnkG (Figure 3g, n=15) and lack NT2-AnkG (Figure 3j, n=15), and pyramidal cell AISs included subgroups labeled by NT2- and NT3-AnkG isoforms in widely varying ratios (Figure 3h, i, k, l). Immunostaining of human neocortical sections using NT1 antibodies revealed no staining of either pyramidal cell or PV interneuron AISs or somata (Supplementary Figure 6d).

Reduced inhibition in *Ank3-1b* mutant mice

Forebrain PV interneurons hypofunction is implicated in epilepsy, many Mendelian neurodevelopmental disorders, and psychiatric illness including BD and schizophrenia(45–48). In mice, heterozygous deletion of *Ank3* exon 1b has been shown to lead to deficient expression of all AnkG isoforms containing NT3(20, 21, 49) and a behavioral phenotype modeling both mania and depression(32), but the mechanisms for this are not clear. Given

the exclusive reliance of PV interneurons on *Ank3* exon 1b isoforms, we analyzed the effects of deficient *Ank3-1b* expression in interneurons, at the behavioral, neuronal network, and cellular levels. Video-EEG telemetry of heterozygous *Ank3-1b*$^{KO/+}$*-PVtom* and homozygous *Ank3-1b*$^{KO/KO}$*-PVtom* mice revealed frequent episodes of generalized 6–7 Hz spike-wave seizures (Figure 4a). Mice exhibited clear behavior arrest at spike-wave onset and resumption of normal behavior immediately following spike-wave offset (Supplementary Information, Movie 2). Homozygous *Ank3-1b*$^{KO/KO}$*-PVtom* mice also experienced rare unprovoked convulsions, and unexplained sudden death not seen in either WT mice or the heterozygous *Ank3* mutants (Figure 4b). In *Ank3-1b*$^{KO/KO}$*-PVtom* mice, repetitive spike-wave discharges of at least 0.5 sec duration occupied 3.9% of the total EEG time; in *Ank3-1b*$^{KO/+}$*-PVtom* mice, these discharges occurred much less frequently (Figure 4c). Mice lacking AnkG specifically in PV interneurons, generated by crossing Flox-*Ank3*(37) and PV cre lines, showed the same dose-dependent epilepsy phenotype seen in the Ank3-1b mutant mice (Figure 4c), providing robust intersectional genetic evidence that the epilepsy was due to loss of NT3-AnkG in PV interneurons. Thalamocortical interactions are implicated in spike-wave epilepsy, and PV interneuron AISs of the thalamic reticular nucleus labeled strongly for NT3-AnkG and not for NT2-AnkG (Supplementary Figure 7).

Loss of Na_V channels at PV interneuron AISs may cause such excitation/inhibition imbalance and epilepsy by diminishing inhibition selectively(50). To assess this, we measured excitatory and inhibitory conductances in the somatosensory barrel cortex under whole cell voltage clamp(51–54). Using a bipolar field electrode placed just below the recorded barrel, we adjusted stimulation intensity to induce a small inhibitory synaptic response in whole cell patched spiny stellate cells at 0 mV in layer IV. We then recorded synaptic currents at −60, −40 and −10 mV, and calculated the underlying excitatory and inhibitory conductances. The G_e/G_i ratio was significantly elevated in the *Ank3-1b*$^{KO/KO}$*-PVtom* compared to *Ank3-1b*$^{+/+}$*-PVtom* mice, due to decrease in G_i but not G_e (Figure 4d).

Ank3-1b$^{KO/KO}$ PV interneurons have diminished excitability

Reduced inhibitory conductance could reflect impaired function at the inhibitory synapse, or loss of interneuron intrinsic excitability. Paradoxically, when we recorded spontaneous inhibitory post-synaptic currents (sIPSCs) from layer IV somatosensory spiny stellate cell, we found mean amplitude was somewhat increased in the mutant mice, and frequency was unchanged (Supplementary 8a–c). Spontaneous excitatory post-synaptic currents were unchanged in *Ank3-1b*$^{KO/KO}$ mice (Supplementary Figure 8d). Thus, the reduced inhibitory conductance we observed does not appear to be due to deficiency of synaptic transmission. By contrast, the threshold extracellular field stimulus strength required to evoke spikes in PV neurons was markedly higher in *Ank3-1b*$^{KO/KO}$*-PVtom* mice than in littermate controls (Figure 5a). Maximal responses were significantly reduced, and the stimulus-response curve was shifted to the right across all intensities tested (Figure 5b, c).

Experiments using direct current injections revealed unchanged passive properties but further evidence of markedly diminished PV interneuron excitability. Input resistance (61.5±6.4 MΩ, n=8 for *Ank3-1b*$^{+/+}$ and 61.9±3.6 MΩ, n=7 for *Ank3-1b*$^{KO/KO}$) and resting membrane potential (−64.33±2.6 mV, n=8 for *Ank3-1b*$^{+/+}$ and −66.6±2.1 mV, n=7 for

Ank3-1b$^{-/-}$) were similar in the two genotypes. However, the mean threshold current for inducing first spikes increased 94% in the mutant mice (264±45.7 pA in *Ank3-1b*$^{KO/KO}$-*PVtom,* and 136±20pA in controls, Figure 5f, Supplementary Figure 9a, b). The AP voltage threshold was depolarized and its half-height duration was lengthened (Figure 5h, i), and the ability to fire repetitively was diminished (Supplementary Figure 9a–c). Steady state membrane potential change induced by different current injection intensities did not differ significantly in *Ank3-1b*$^{KO/KO}$ compared to *Ank3-1b*$^{+/+}$ (Supplementary Figure 9e). Although first spike amplitudes were not significantly smaller in *Ank3-1b*$^{KO/KO}$ compared to controls, latencies were longer (Supplementary Figure 9f, g). Reflecting these changes, AP phase plots from mutant mice exhibit clear changes in threshold, ascent, and repolarization (Figure 5g). In combination, extracellular stimulation and direct current injection experiments show that PV cell excitability in *Ank3-1b*$^{KO/KO}$-*PVtom* mice is profoundly reorganized, and very markedly reduced.

DISCUSSION

Several independent genome-wide association studies (GWAS) have implicated variation near the 5′ non-coding region of *ANK3* in BD(14–19), but the underlying biological mechanisms are challenging to analyze and have been obscure. Taken together, the results shown here provide a compelling new explanation. We find that forebrain AnkG proteins include two major isoform families, defined by alternative promoters, first exons, and N-termini, which make largely opposing contributions to neuronal circuit excitability. Inhibitory PV neurons rely exclusively on NT3 isoforms, whereas excitatory principal cells express either NT2 exclusively or combinations of NT2 and NT3. This previously unappreciated subdivision of AnkG function is important, since PV interneurons play critical roles in brain microcircuits, including feedforward and feedback inhibition, gamma oscillations, and control of the slope (or gain) of input/output relationships, (34–36). Given the role of NT3-AnkG in PV cells, we studied heterozygous NT3-AnkG knockout mice previously shown to exhibit behavioral abnormalities modeling mania and depression(21), and in mice homozygous for the same deletion. The mice have epilepsy with gene-dosage-related severity. The homozygotes have very frequent seizures and sudden death. These phenotypes reflect deficient expression in PV interneurons, since they also could be produced by deletion of *Ank3* we restricted to PV neurons using Cre-lox. Hippocampal PV interneurons deficient in NT3-AnkG have a proportional loss in Na_V channels at the AIS. We found that the CA1 PV AIS was approximately 20 um long cell The AIS distal tip determined by Na_V and AnkG immunolabeling corresponds closely to the site of AP initiation mapped electrophysiologically(24). Our staining and recording results show that NT3-AnkG null neocortical PV cells both lack the requisite AIS channels and associated protein complexes, and exhibit dramatically impaired intrinsic excitability, manifest by increased synaptic stimulation and current injection required for firing, increased first latencies, depolarized AP thresholds, reduced firing rates, lengthened AP duration, and a loss in AP height with sustained firing.

The severe early-onset circuit disorder exhibited by global, constitutive homozygous NT3-AnkG knockout mice and PV neuron-specific AnkG-deleted mice represents one extreme along a spectrum of brain NT2/NT3 balance. Indeed a recent study identified 3 siblings with

epilepsy and severe neurodevelopmental impairment due to homozygous truncating *ANK3* mutation(55). Our result suggest that the modest effects of *ANK3* variation observed in BD GWASs could arise in part from imbalances of AnkG isoform expression that are smaller, and/or restricted in brain region or developmental stage. Recently, initial human mRNA analyses have correlated reduced expression of NT3 isoforms with increased risk of BD(21), and reduced NT2 isoform expression in adolescence and early adulthood with protection from BD and schizophrenia(33). More comprehensive analysis of human mRNA and protein levels, and parallel study in animals using behavioral paradigms modulating gene expression and protein function (e.g., stress), are next steps for elucidating AnkG-related interneuronopathy. One recent study screened individuals diagnosed with BD and controls for de novo variants in exon 37, near another *ANK3* SNP(56). Rare variants within conserved coding(33) and non-coding regions controlling NT3 and NT2 expression represent an appealing candidate mechanism for BD. Existing databases of genotyped BD patients from previous collaborative GWAS should be interrogated to learn if epilepsy is more common in individuals bearing *ANK3* SNPs known to confer BD risk. The GWAS approach has been less extensively exploited in epilepsy than in psychiatric disorders, and it will be interesting to learn whether future epilepsy GWASs implicate *ANK3*(57). A full view of how the expression ratios of AnkG isoforms and their channel ligands(23–26) are altered in BD and epilepsy promises to reveal specific new candidate therapeutic targets. Thinking about mood disorders and epilepsy is often segregated into psychiatric and neurological perspectives, and the mechanisms underlying comorbidity between these diseases have not been adequately explored. The current work provides an example how unbiased human genetic studies can illuminate unforeseen connections between disease categories.

Supplementary Material

Refer to Web version on PubMed Central for supplementary material.

Acknowledgments

We thank Mia Cooper for excellent technical assistance, Vann Bennett for generous gifts of AnkG antibodies, cDNA, and transgenic mouse lines, and members of the Cooper lab, Matthew Rasband and Rodney Samaco for helpful discussions. This study was supported by NIH R01 NS49119.

References

1. Krishnan V, Nestler EJ. The molecular neurobiology of depression. Nature. 2008; 455:894–902. [PubMed: 18923511]
2. England MJ, Liverman CT, Schultz AM, Strawbridge LM. Epilepsy across the spectrum: promoting health and understanding. A summary of the Institute of Medicine report. Epilepsy behav. 2012; 25:266–276. [PubMed: 23041175]
3. Craddock N, Sklar P. Genetics of bipolar disorder. Lancet. 2013; 381:1654–1662. [PubMed: 23663951]
4. Mula M, Sander JW. Suicide risk in people with epilepsy taking antiepileptic drugs. Bipolar Disord. 2013; 15:622–627. [PubMed: 23755740]
5. Tondo L, Pompili M, Forte A, Baldessarini RJ. Suicide attempts in bipolar disorders: comprehensive review of 101 reports. Acta Psychiatr Scand. 2016; 133:174–186. [PubMed: 26555604]

6. Hesdorffer DC, Ishihara L, Mynepalli L, Webb DJ, Weil J, Hauser WA. Epilepsy, suicidality, and psychiatric disorders: a bidirectional association. Ann Neurol. 2012; 72:184–191. [PubMed: 22887468]
7. Lau C, Ettinger AB, Hamberger S, Fanning K, Reed ML. Do mood instability symptoms in epilepsy represent formal bipolar disorder? Epilepsia. 2012; 53:e37–40. [PubMed: 22220741]
8. Garcia-Morales I, de la Pena Mayor P, Kanner AM. Psychiatric comorbidities in epilepsy: identification and treatment. Neurologist. 2008; 14:S15–25. [PubMed: 19225366]
9. Wotton CJ, Goldacre MJ. Record-linkage studies of the coexistence of epilepsy and bipolar disorder. Soc Psychiatry Psychiatr Epidemiol. 2014; 49:1483–1488. [PubMed: 24638891]
10. Adelow C, Andersson T, Ahlbom A, Tomson T. Hospitalization for psychiatric disorders before and after onset of unprovoked seizures/epilepsy. Neurology. 2012; 78:396–401. [PubMed: 22282649]
11. Noebels JL. Single-Gene Determinants of Epilepsy Comorbidity. Cold Spring Harb Perspect Med. 2015; 5:1–13.
12. Uher R. Gene-environment interactions in severe mental illness. Front Psychiatry. 2014; 5:48. [PubMed: 24860514]
13. Ioannidis JP, Thomas G, Daly MJ. Validating, augmenting and refining genome-wide association signals. Nat Rev Genet. 2009; 10:318–329. [PubMed: 19373277]
14. Ferreira MA, O'Donovan MC, Meng YA, Jones IR, Ruderfer DM, Jones L, et al. Collaborative genome-wide association analysis supports a role for ANK3 and CACNA1C in bipolar disorder. Nat Genet. 2008; 40:1056–1058. [PubMed: 18711365]
15. Schulze TG, Detera-Wadleigh SD, Akula N, Gupta A, Kassem L, Steele J, et al. Two variants in Ankyrin 3 (*ANK3*) are independent genetic risk factors for bipolar disorder. Mol Psychiatry. 2009; 14:487–491. [PubMed: 19088739]
16. Scott LJ, Muglia P, Kong XQ, Guan W, Flickinger M, Upmanyu R, et al. Genome-wide association and meta-analysis of bipolar disorder in individuals of European ancestry. Proc Natl Acad Sci U S A. 2009; 106:7501–7506. [PubMed: 19416921]
17. Tesli M, Koefoed P, Athanasiu L, Mattingsdal M, Gustafsson O, Agartz I, et al. Association analysis of *ANK3* gene variants in nordic bipolar disorder and schizophrenia case-control samples. Am J Med Genet B Neuropsychiatr Genet. 2011; 156:969–974.
18. Sklar P, Ripke S, Scott LJ, Andreassen OA, Cichon S, Craddock N. Large-scale genome-wide association analysis of bipolar disorder identifies a new susceptibility locus near *ODZ4*. Nat Genet. 2011; 43:977–983. [PubMed: 21926972]
19. Muhleisen TW, Leber M, Schulze TG, Strohmaier J, Degenhardt F, Treutlein J, et al. Genome-wide association study reveals two new risk loci for bipolar disorder. Nat Commun. 2014; 5:3339. [PubMed: 24618891]
20. Zhou D, Lambert S, Malen PL, Carpenter S, Boland LM, Bennett V. AnkyrinG is required for clustering of voltage-gated Na channels at axon initial segments and for normal action potential firing. J Cell Biol. 1998; 143:1295–1304. [PubMed: 9832557]
21. Rueckert EH, Barker D, Ruderfer D, Bergen SE, O'Dushlaine C, Luce CJ, et al. Cis-acting regulation of brain-specific ANK3 gene expression by a genetic variant associated with bipolar disorder. Mol Psychiatry. 2012; 18:1–8.
22. Pan Z, Kao T, Horvath Z, Lemos J, Sul JY, Cranstoun SD, et al. A common ankyrin-G-based mechanism retains KCNQ and NaV channels at electrically active domains of the axon. J Neurosci. 2006; 26:2599–2613. [PubMed: 16525039]
23. Battefeld A, Tran BT, Gavrilis J, Cooper EC, Kole MH. Heteromeric Kv7.2/7. 3 channels differentially regulate action potential initiation and conduction in neocortical myelinated axons. J Neurosci. 2014; 34:3719–3732. [PubMed: 24599470]
24. Hu H, Jonas P. A supercritical density of Na(+) channels ensures fast signaling in GABAergic interneuron axons. Nat Neurosci. 2014; 17:686–693. [PubMed: 24657965]
25. Schwarz JR, Glassmeier G, Cooper EC, Kao TC, Nodera H, Tabwena D, et al. Evidence that KCNQ channels mediate I_{Ks}, a slow subthreshold K^+ current in the rat node of Ranvier. J Physiol. 2006; 573:1–17. [PubMed: 16543261]

26. Xu M, Cooper EC. An Ankyrin-G N-terminal Gate and Protein Kinase CK2 Dually Regulate Binding of Voltage-gated Sodium and KCNQ2/3 Potassium Channels. J Biol Chem. 2015; 290:16619–16632. [PubMed: 25998125]
27. Noebels J. Pathway-driven discovery of epilepsy genes. Nat Neurosci. 2015; 18:344–350. [PubMed: 25710836]
28. Kay HY, Greene DL, Kang S, Kosenko A, Hoshi N. M-current preservation contributes to anticonvulsant effects of valproic acid. J Clin Invest. 2015; 125:3904–3914. [PubMed: 26348896]
29. Geddes JR, Miklowitz DJ. Treatment of bipolar disorder. Lancet. 2013; 381:1672–1682. [PubMed: 23663953]
30. Kent WJSC, Furey TS, Roskin KM, Pringle TH, Zahler AM, Haussler D. The human genome browser at UCSC. Genome Res. 2002; 12:996–1006. [PubMed: 12045153]
31. Quinn EM, Hill M, Anney R, Gill M, Corvin AP, Morris DW. Evidence for cis-acting regulation of ANK3 and CACNA1C gene expression. Bipolar Disord. 2010; 12:440–445. [PubMed: 20636642]
32. Leussis MP, Berry-Scott EM, Saito M, Jhuang H, de Haan G, Alkan O, et al. The ANK3 bipolar disorder gene regulates psychiatric-related behaviors that are modulated by lithium and stress. Biol Psychiatry. 2013; 73:683–690. [PubMed: 23237312]
33. Hughes T, Hansson L, Sonderby IE, Athanasiu L, Zuber V, Tesli M, et al. A Loss-of-Function Variant in a Minor Isoform of ANK3 Protects Against Bipolar Disorder and Schizophrenia. Biol Psychiatry. 2016; 80:323–330. [PubMed: 26682468]
34. Hu H, Gan J, Jonas P. Interneurons. Fast-spiking, parvalbumin(+) GABAergic interneurons: from cellular design to microcircuit function. Science. 2014; 345:1255–1263. [PubMed: 25214598]
35. Wilson NR, Runyan CA, Wang FL, Sur M. Division and subtraction by distinct cortical inhibitory networks in vivo. Nature. 2012; 488:343–348. [PubMed: 22878717]
36. Atallah BV, Bruns W, Carandini M, Scanziani M. Parvalbumin-expressing interneurons linearly transform cortical responses to visual stimuli. Neuron. 2012; 73:159–170. [PubMed: 22243754]
37. Jenkins PM, Vasavda C, Hostettler J, Davis JQ, Abdi K, Bennett V. E-cadherin polarity is determined by a multifunction motif mediating lateral membrane retention through ankyrin-G and apical-lateral transcytosis through clathrin. J Biol Chem. 2013; 288:14018–14031. [PubMed: 23530049]
38. Maheshwari A, Nahm WK, Noebels JL. Paradoxical proepileptic response to NMDA receptor blockade linked to cortical interneuron defect in stargazer mice. Front Cell Neurosci. 2013; 7:156. [PubMed: 24065886]
39. Paxinos, G., Franklin, K. The Mouse Brain in Stereotaxic Coordinates. San Diego, California: Academic Press; 1997.
40. Agmon A, Connors BW. Thalamocortical responses of mouse somatosensory (barrel) cortex in vitro. Neuroscience. 1995; 41:365–379.
41. Agmon A, Yang LT, Jones EG, O'Dowd DK. Topological precision in the thalamic projection to neonatal mouse barrel cortex. J Neurosci. 1995; 15:549–561. [PubMed: 7823163]
42. Zhang Z, Sun QQ. Development of NMDA NR2 subunits and their roles in critical period maturation of neocortical GABAergic interneurons. Dev Neurobiol. 2011; 71:221–245. [PubMed: 20936660]
43. Kordeli E, Lambert S, Bennett V, Ankyrin G. A new ankyrin gene with neural-specific isoforms localized at the axonal initial segment and node of Ranvier. J Biol Chem. 1995; 270:2352–2359. [PubMed: 7836469]
44. Townsend J, Altshuler LL. Emotion processing and regulation in bipolar disorder: a review. Bipolar Disord. 2012; 14:326–339. [PubMed: 22631618]
45. Zhang ZJ, Reynolds GP. A selective decrease in the relative density of parvalbumin-immunoreactive neurons in the hippocampus in schizophrenia. Schizophr Res. 2002; 55:1–10. [PubMed: 11955958]
46. Marin O. Interneuron dysfunction in psychiatric disorders. Nat Rev Neurosci. 2012; 13:107–120. [PubMed: 22251963]
47. Maheshwari A, Noebels JL. Monogenic models of absence epilepsy: windows into the complex balance between inhibition and excitation in thalamocortical microcircuits. Prog Brain Res. 2014; 213:223–252. [PubMed: 25194492]

48. Chao HT, Chen H, Samaco RC, Xue M, Chahrour M, Yoo J, et al. Dysfunction in GABA signalling mediates autism-like stereotypies and Rett syndrome phenotypes. Nature. 2010; 468:263–269. [PubMed: 21068835]

49. Kordeli E, Lambert S, Bennett V, Ankyrin G. A new ankyrin gene with neural-specific isoforms localized at the axonal initial segment and node of Ranvier. J Biol Chem. 1995; 270:2352–2359. [PubMed: 7836469]

50. Ogiwara I, Miyamoto H, Morita N, Atapour N, Mazaki E, Inoue I, et al. Na(v)1. 1 localizes to axons of parvalbumin-positive inhibitory interneurons: a circuit basis for epileptic seizures in mice carrying an Scn1a gene mutation. J Neurosci. 2007; 27:5903–5914. [PubMed: 17537961]

51. Borg-Graham LJ, Monier C, Fregnac Y. Visual input evokes transient and strong shunting inhibition in visual cortical neurons. Nature. 1998; 393:369–373. [PubMed: 9620800]

52. Zhang Z, Jiao YY, Sun QQ. Developmental maturation of excitation and inhibition balance in principal neurons across four layers of somatosensory cortex. Neuroscience. 2011; 174:10–25. [PubMed: 21115101]

53. Cruikshank SJ, Lewis TJ, Connors BW. Synaptic basis for intense thalamocortical activation of feedforward inhibitory cells in neocortex. Nat Neurosci. 2007; 10:462–468. [PubMed: 17334362]

54. Sun QQ, Huguenard JR, Prince DA. Barrel cortex microcircuits: thalamocortical feedforward inhibition in spiny stellate cells is mediated by a small number of fast-spiking interneurons. J Neurosci. 2006; 26:1219–1230. [PubMed: 16436609]

55. Iqbal Z, Vandeweyer G, van der Voet M, Waryah AM, Zahoor MY, Besseling JA, et al. Homozygous and heterozygous disruptions of *ANK3*: at the crossroads of neurodevelopmental and psychiatric disorders. Hum Mol Genet. 2013; 22:1960–70. [PubMed: 23390136]

56. Doyle GA, Lai AT, Chou AD, Wang MJ, Gai X, Rappaport EF, et al. Re-sequencing of ankyrin 3 exon 48 and case-control association analysis of rare variants in bipolar disorder type I. Bipolar Disord. 2012; 14:809–21. [PubMed: 22966748]

57. Poduri A. Meta-analysis revives genome-wide association studies in epilepsy. Epilepsy Curr. 2015; 15:122–3. [PubMed: 26316846]

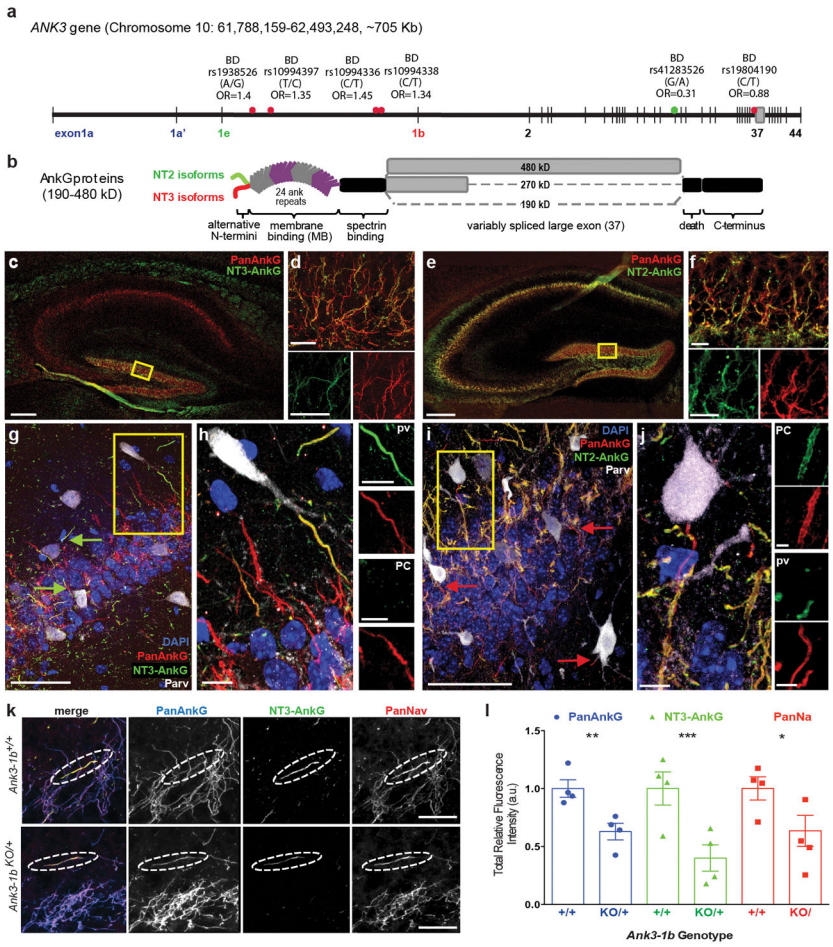

Figure 1.

NT3-AnkG localizes Nav channels to the AIS of PV-interneurons. (**a**) *ANK3* gene map labeled with BD-associated SNPs (*) and a BD-protective SNP(*). Alternative exons encoding NT1 (exon 1a and 1a′), NT2 (exon 1e) and NT3 (exon 1b) are labeled. (**b**) Brain AnkG protein isoforms generated by alternative first exon use (NT2 and NT3) and alternative splicing of the large exon (190, 270 and 480 kD). (**c–j**) NT2-AnkG and NT3-AnkG have distinct cell type specific expression in the hippocampus. (**c, e**) Low magnification: CA regions appear to contain only NT2-AnkG, while the dentate gyrus (DG) labels for both NT2- and NT3-AnkG. (**d, f**) Higher magnification (boxed regions from a, c): DG cells express NT2-AnkG always and NT3 variably. (**f, i**) High magnification: CA3 shows labeling of PV interneuron (PV; white) AISs by only NT3 (arrows). CA3 pyramidal cells (PC) express only NT2-AnkG. (**h, j**) High magnification (boxed regions from **g**, **i**): CA3 PVs express only NT3 and PCs only NT2 (**k–l**) Heterozygous *Ank3* exon 1b deletion proportionally reduces AnkG and Na_V channel labeling at AISs of CA1 PV interneurons. (**k**) CA1 images from *Ank3-1b*$^{KO/+}$ and WT mice, acquired under identical conditions. (**l**) Fluorescence intensity at PV AISs is significantly reduced for PanAnkG (p=0.0009), NT3-AnkG (p<0.0001) and PanNa_V (p=0.0049) in *Ank3-1b*$^{KO/+}$ compared WT. Scales: **c, e**: 100 μm; **d, f, h, j**: 10 μm; **g, i**: 50 μm; **d, f** subpanels: 5μm; **h, j** subpanels: 2 μm, **k**: 10 μm.

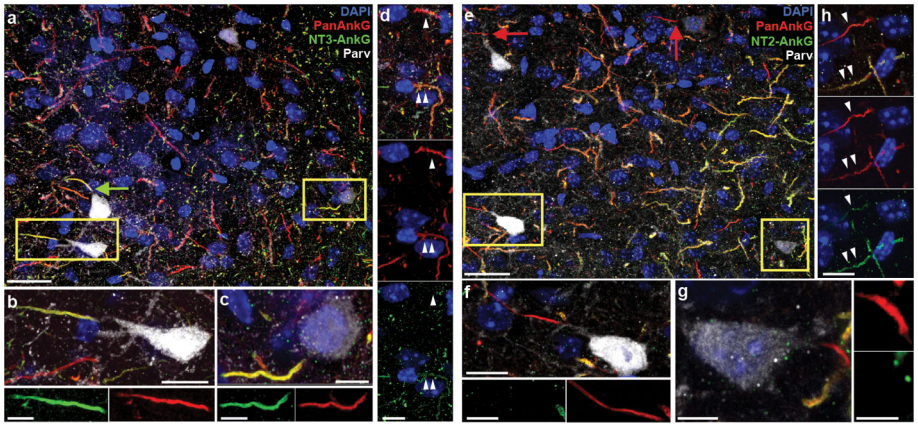

Figure 2.

PV-interneurons in the basolateral amygdala (bla) express only NT3-AnkG. (**a**) BLA section labeled by the three indicated antibodies and DAPI. PV interneuron AISs (green arrows) appear yellow due to colabeling by NT3-AnkG (green) and all-AnkG (red) antibodies. Both strongly and weakly PV labeled interneurons (yellow boxes) express NT3. (**b–c**) Higher magnification views of two strongly NT3 labeled boxed cells from **a** exhibit strong (**b**) and light (**c**) PV labeling. (**d**) Two neighboring non-PV neurons: the upper AIS (single arrowhead) lacks detectable NT3 staining; the lower (double arrowheads) shows light NT3 labeling. Upper panel: merge; middle: NT2; lower: NT3. (**e**) AISs of PV interneurons (red arrows) are not labeled by NT2; both strongly and weakly PV labeled interneurons (yellow boxes) lack NT2. (**f–g**) Higher magnification views of two boxed cells from **e,** strongly (**f**) and lightly (**g**) PV labeled. Neither AIS stains for NT2. **h,** Two neighboring non-PV neurons: the upper AIS (single arrowhead) has light NT2 staining; the lower (double arrowheads) shows strong NT2 labeling. Upper panel: merge; middle: NT2; lower: NT3. Scales: **a, e:** 25 μm; **b–d, g–h:** 5 μm.

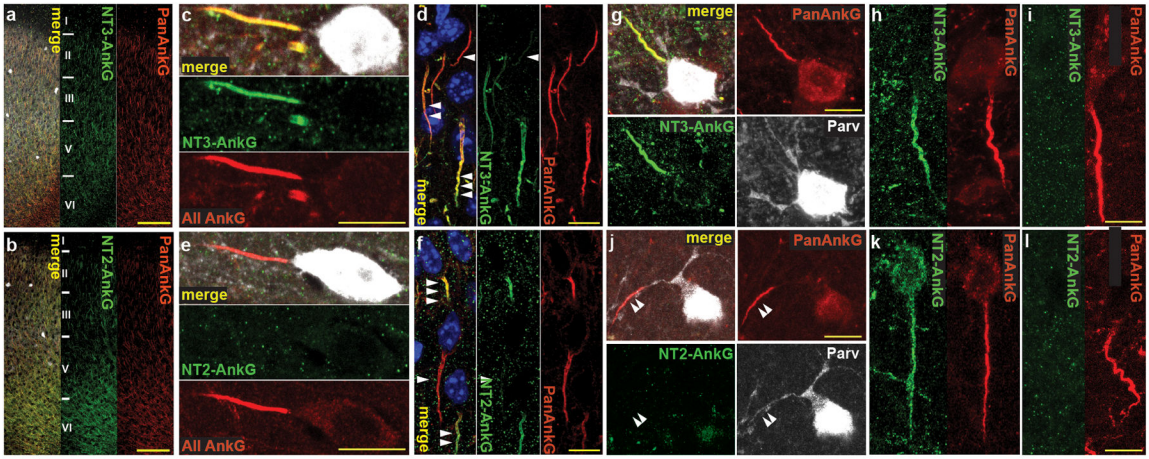

Figure 3.

Cell type specific NT2-AnkG and NT3- AnkG expression is conserved in mouse and human cortex. (**a–f**) Mouse anterior cingulate cortex: (**a–b**) Widespread NT3 (**a**: green) and NT2 (**b**: green) labeling of neurons in area Cg2/24b. (**c, e**) High magnification: exclusive NT3 expression neocortical PV interneurons at AISs. (**d**) PCs show varied NT3 expression: weak NT3 labeling (◀), moderate NT3 labeling (◀◀)and strong NT3 labeling (◀◀◀). (**f**) PCs show varied NT2 expression: lack NT2 labeling (◀), moderate NT2 labeling ◀◀) and strong NT2 labeling (◀◀◀). (**g–l**) NT2 and NT3 expression pattern is conserved in human. (**g, j**) Human PV interneurons (frontal lateral neocortex) exclusively express NT3. Arrowheads in **j** mark a PV interneuron AIS lacking NT2 staining. (**h–i, k–l**) Pyramidal neurons variably express the two isoforms. Scales: **a, b:** 100 μm; **c–f, g–l**: 10 μm.

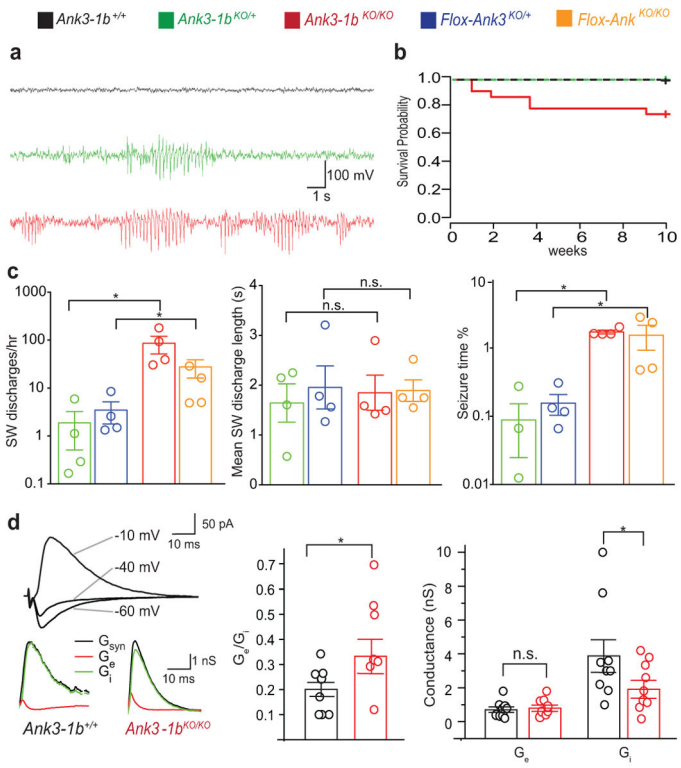

Figure 4.

Ank3 exon 1b deletion results in epilepsy and reduced cortical network inhibition. (**a**) Representative EEG recordings showing repetitive spike-wave (SW) discharges and seizures in *Ank3-1b*$^{KO/+}$*-PVtom* and *Ank3-1b*$^{KO/KO}$*-PVtom* mice, not present in controls. (**b**) *Ank3-1b*$^{KO/KO}$*-PVtom* survival to P28 probability (75%, n=25) is significantly decreased (p=0.0284) compared to *Ank3-1b*$^{KO/+}$*-PVtom* (n=13) and WT (n=15). (**c**) *Ank3-1b*$^{KO/KO}$*-PVtom* mice have significantly more SW discharges per hour (log scale, P=0.0266), and spend more time in SW activity (log scale, P=0.0266), but similar average duration of SW discharges, compared to *Ank3-1b*$^{KO/+}$*-PVtom* mice. This likely is due to effects on PV neurons, as *Flox-Ank3*$^{KO/KO}$ also have more discharges per hour (P=0.0266) and experience more SW activity than *Flox-Ank3*$^{KO/+}$ (P=0.0266). (**d**) Top, evoked synaptic current under different holding potentials (−60, −40, −10mV). Bottom, the compound synaptic conductance G_{syn}, excitatory conductance G_e, and inhibitory conductance, G_i. The G_e/G_i ratio is significantly higher in *Ank3-1b*$^{KO/KO}$*-PVtom* mice (0.39±0.2, n=7) compared to control (0.2±0.1, n=9, P=0.02), due to decreased G_i in KO (2.05±1.4, n=9) compared to control (3.9±2.9, n=7, P=0.04).

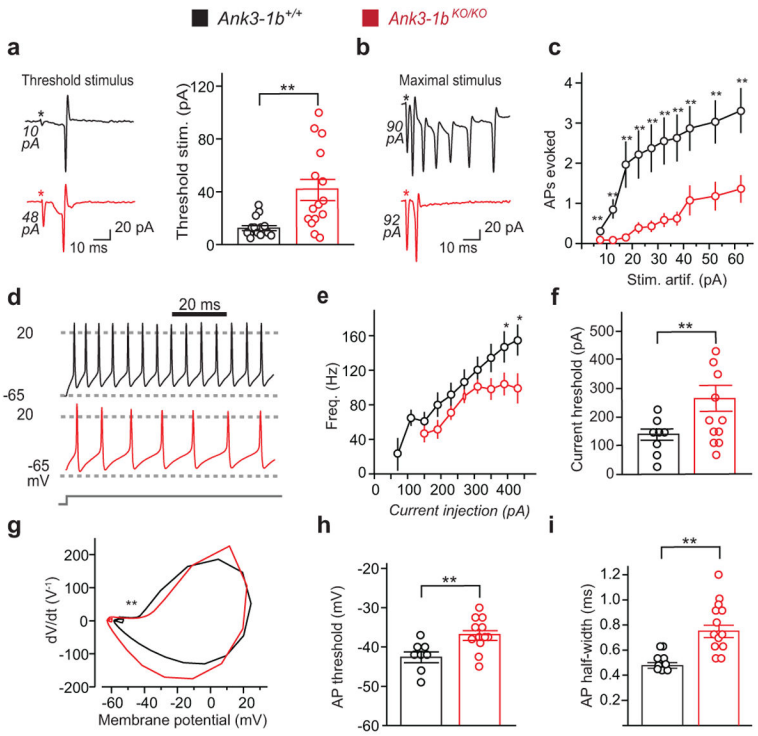

Figure 5.

Ank3-1b KO mouse PV interneurons are less responsive due to reduced intrinsic excitability. (**a-c**) In cell attached recordings, *Ank3-1b*$^{KO/KO}$*-PVtom* PV cells fire less than controls in response to extracellular field stimulation. The stimulation artifact is proportional to stimulation amplitude and is labeled (*) for each trace. (**a**) The threshold stimulus required to evoke a single AP is markedly increased in *Ank3-1b*$^{KO/KO}$*-PVtom* PV cells (41.7±30.5 pA vs. control: 12.9±7.2 pA, n=16; P=0.001). (**b**) Representative traces illustrate reduced maximal firing response of mutant cells (note large stimulation artifact amplitudes). (**c**) Significantly reduced excitability in *Ank3-1b*$^{KO/KO}$*-PVtom* PV cells (n=16; P=0.03, 0.003, 0.003, 0.005, 0.003, 0.003, 0.002, 0.007, 0.004, and 0.003) compared to control (n=14). (**d–i**) *Ank3-1b*$^{KO/KO}$*-PVtom* PV cells fire less than controls in response to current injection (whole cell recordings). (**d**) Representative recordings of AP trains show reduced firing responses in a mutant cell compared to WT control cell (injection current, 230 pA). (**e**) Firing frequency is significantly decreased in *Ank3-1b*$^{KO/KO}$*-PVtom* mice (n=9; P=0.19, 0.07, 0.12, 0.19, 0.14, 0.05, 0.03, 0.02 for each current) compared to control (n=7). (**f**) Threshold current is significantly increased (n=11; P=0.016). (**g**) Representative AP phase plots, with depolarized ascending phase (**) of mutant indicated. (**h**) AP voltage threshold (n = 11 mutant; 8 WT, P=0.004) and **I**, half-width (n = 13; P=0.004) are significantly increased in *Ank3-1b*$^{KO/KO}$*-PVtom* mice compared to control (n = 9).